Experimental Demonstration of Efficient Harmonic Generation via Surface Plasma Compression with Lasers

B. Y. Li,[1,2,3] F. Liu,[1,3,*] M. Chen,[1,3,†] F. Y. Wu,[1,3] J. W. Wang,[4] L. Lu,[1,3] J. L. Li,[1,3] X. L. Ge,[1,3] X. H. Yuan,[1,3] W. C. Yan,[1,3] L. M. Chen,[1,3] Z. M. Sheng,[1,2,3] and J. Zhang[1,2,3]

[1]*Key Laboratory for Laser Plasmas (Ministry of Education), School of Physics and Astronomy, Shanghai Jiao Tong University, Shanghai 200240, China*

[2]*Tsung-Dao Lee Institute, Shanghai Jiao Tong University, Shanghai 200240, China*

[3]*Collaborative Innovation Center of IFSA (CICIFSA), Shanghai Jiao Tong University, Shanghai 200240, China*

[4]*State Key Laboratory of High Field Laser Physics, Shanghai Institute of Optics and Fine Mechanics, Chinese Academy of Sciences, Shanghai 201800, China*

(Received 16 January 2022; revised 9 April 2022; accepted 24 May 2022; published 14 June 2022)

The efficiency of high-order harmonic generation from a relativistic laser interacting with solid targets depends greatly on surface plasma distribution. The usual method of enhancing efficiency involves tuning the plasma scale length carefully by improving the laser contrast. Here, we experimentally demonstrate that efficient harmonics can be achieved directly by compressing large-scale surface plasma via the radiation pressure of a circularly polarized normally incident prepulse. The harmonic generation efficiency obtained by this method is comparable to that obtained with optimized plasma scale length by high-contrast lasers. Our scheme does not rely on high-contrast lasers and is robust and easy to implement. Thus, it may pave a way for the development of intense extreme ultraviolet sources and future applications with high repetition rates.

DOI: 10.1103/PhysRevLett.128.244801

High-order harmonic generation (HHG) using ultrashort lasers interacting with solid targets through a relativistically oscillating mirror (ROM) [1–3] is a promising method for developing advanced extreme ultraviolet (EUV) or x-ray sources without laser intensity limitations. Such light sources can be used for atom-molecular dynamic diagnosis [4], coherent diffraction imaging [5], attosecond pulse generation [6], seeding free-electron lasers [7], and achieving extremely strong fields [8]. Since harmonics from ROM are produced by the coherent motion of electrons around the target surface, the density distribution of surface plasma is an important factor that affects the generation efficiency. When a laser with amplified spontaneous emission and prepulses irradiates the target, surface preplasma is created with certain scale lengths $L = n_p/(dn_p/dx)$, where n_p is the plasma density. Extensive studies have proven that L should be well controlled for efficient HHG [9–11]. For a large L, the laser spectrum will be modified in the underdense preplasma by the parametric instabilities [11] and self-phase modulation [12]; meanwhile the thickness of the oscillating electron sheet contributing to harmonic generation is enlarged. The above two factors will change the spectrum and efficiency of harmonic radiation.

The high contrast (HC) of lasers is an essential prerequisite for suppressing preplasma formation in HHG [13,14]. However, as the plasma scale length decreases, the laser fields are significantly attenuated in the skin layer near the critical surface [15], while the space charge separation fields between the electrons and ions become stronger because of the density increase of the laser-driven electrons. Owing to these effects, it is hard for the laser to drive surface electron oscillations with a large relativistic parameter γ_e for efficient HHG when $L \to 0$ [16]. Both experiments and simulations show that the generation efficiency of ROM harmonics should be optimized to approximately $L \sim \lambda/10$ [10,11]. To achieve such a scale length, laser pulses with extremely high temporal contrasts, in combination with a prepulse to precisely tune the scale length, are routinely required in experiments [10,11], which is a significant challenge for high-power laser systems.

For efficient HHG, surface plasma with a sharp front and a few times the critical density is preferred. Our previous theoretical study showed that such a density distribution has three advantages for HHG [17]. First, the laser interacts directly with the overdense plasma without a long underdense preplasma tail; therefore, the motion coherence of surface electrons for HHG is remarkably improved. Second, with the moderate overdense plasma surface, the laser can drive surface electrons to oscillate with larger γ_e for a more efficient generation of higher-order harmonics. Finally, HHG does not rely on high-contrast lasers.

In this Letter, we experimentally demonstrate efficient HHG via the compression of the large-scale surface plasma to a sharply truncated profile with an overcritical density. Surface plasma compression is achieved by applying the radiation pressure of a circularly polarized normally

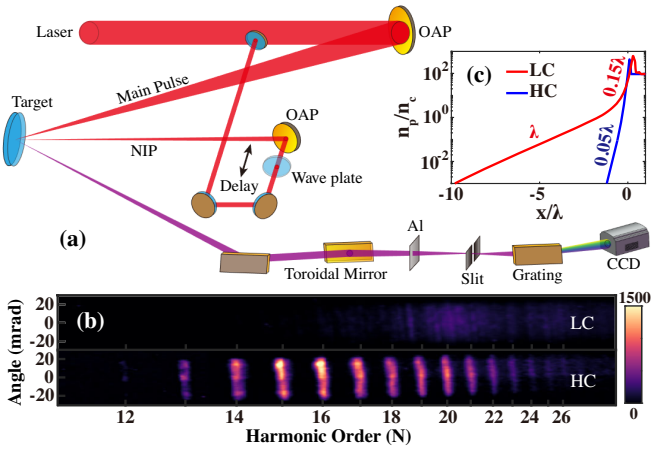

FIG. 1. (a) Experimental setup for HHG and measurements. The red and violet beams represent the lasers and high-order harmonics, respectively. The harmonics are horizontally dispersed and vertically imaged by a toroidal grating onto a charge-coupled device (CCD). (b) Experimental harmonic images obtained using LC and HC lasers. (c) Preplasma profiles calculated using MULTI-IFE for LC and HC lasers, where $n_c = 1.75 \times 10^{21}$ cm^{-3} is the critical plasma density.

incident prepulse (NIP), which requires a very small fraction of the low-contrast (LC) laser energy. The harmonic generation efficiency from the compressed plasma is comparable to that obtained at the optimum scale length with a high-contrast laser.

The experiment was carried out on the 200 TW laser ($\lambda = 800$ nm, $\tau = 30$ fs) facility at Shanghai Jiao Tong University. The laser system delivered pulses with a beam energy of 3 J after compression and a picosecond contrast of 10^{-9} at 10 ps before the main pulses. The initial laser contrast was not sufficiently high to produce an $L \sim \lambda/10$ level preplasma. By using a single plasma mirror, the laser contrast was improved to 10^{-11} [18,19]. The laser can easily switch from high contrast to low contrast when the plasma mirror is bypassed. The experimental setup is shown in Fig. 1(a). The laser beam was focused onto the surface of the fused silica targets with an incident angle of 45° by an $f/4$ off-axis parabolic (OAP) mirror. The laser spot size was measured to be 7×7 μm^2; therefore, the calculated peak intensity was 4×10^{19} W/cm^2 for the LC laser and 2.8×10^{19} W/cm^2 for the HC laser, considering the 30% laser energy loss by the plasma mirror [24].

Harmonic radiation in the laser reflection direction was collected by a gold-coated mirror and focused by a toroidal mirror onto the entrance slit of an imaging EUV flat-field spectrometer. A 250-nm-thick aluminum foil was placed before the slit to block the reflected laser beam. The spectrometer can spatially and spectrally resolve the radiation, with a detection angle of ±20 mrad and a spectral range of 17–70 nm. Figure 1(b) shows the raw harmonic images obtained using laser pulses with different contrasts. No harmonics could be observed for the LC laser, whereas clear and intense harmonics were produced by the HC laser.

We used the one-dimensional hydrodynamic code MULTI-IFE [25] to calculate the preplasma formation using the laser contrast trace measured by a third-order autocorrelator. The target was initially weakly ionized SiO_2. Figure 1(c) shows the simulated preplasma density distributions with different laser contrasts, where the electrons and ions have the same profile. A very steep preplasma with $L = 0.05\lambda$ is created by the HC laser. The LC laser creates a longer preplasma of $L = \lambda$ followed by a relatively short preplasma of $L = 0.15\lambda$. The plasma structure with two density scale lengths was also found in Ref. [26]. As the appearance of the low-density preplasma with $L \sim \lambda$, high-order harmonics cannot be efficiently generated by the LC laser.

To remove the low-density preplasma detrimental to HHG, we introduced a NIP to compress the preplasma created by the LC laser. As shown in Fig. 1(a), a small reflection mirror was inserted to produce the NIP containing 6% of the laser energy. This beam was first sent to a delay line, which can adjust the t_{delay} of NIP relative to the main pulse within ±80 ps. To avoid heating the preplasma and producing electromagnetic instabilities at the target surface, a quarter-wave plate was used to convert the laser pulse from p polarization to circular polarization. Finally, an $f/7$ OAP focused the beam normally onto the target surface with a spot size of 20×14 μm^2, producing a peak intensity of 2×10^{17} W/cm^2. Figure 2(a) shows the measured harmonics generated by the LC laser with NIP at $t_{\mathrm{delay}} = -1.6$ ps. The reproducibility of HHG is presented in the Supplemental Material [19]. The harmonic intensities generated by the LC + NIP lasers were even higher than those obtained by the HC laser. In this case, the efficient HHG indicates that the low-density preplasma with $L \sim \lambda$ shown in Fig. 1(c) was removed by the NIP compression. Figure 2(c) compares the experimental harmonic spectra under different conditions. It can be observed that the harmonics at orders $N > 15$th were significantly enhanced and showed a plateau profile in the LC + NIP case. In contrast, the harmonic intensity of the HC laser case declines monotonically and rapidly as the harmonic order increases.

We also compared the optimized harmonic generation by the HC laser with that by the LC + NIP lasers. For the HHG in our HC laser case, the preplasma scale length $L = 0.05\lambda$ is shorter than the optimum scale length according to previous studies [10,11]. To optimize the HHG in this case, we introduced a prepulse coaxially propagating with the main pulse to tune the plasma scale length [19], similar to the methods used in Refs. [10,11]. The energy ratio of the coaxial prepulse to the main pulse was 1/400, and its temporal delay with respect to the main pulse t_{delay} could be finely adjusted within ±5 ps. The coaxial prepulse ionized the target surface such that the density scale length of the

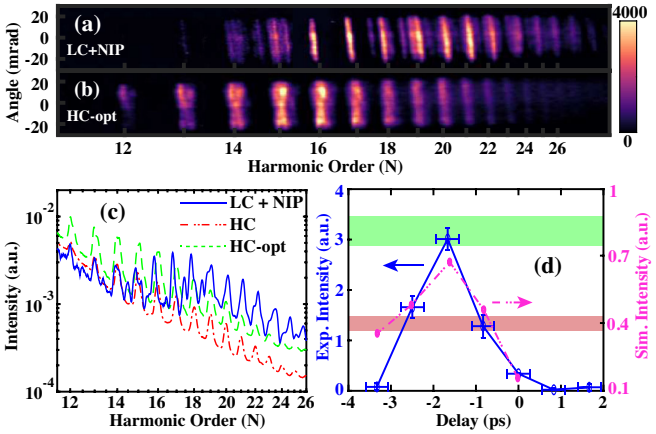

FIG. 2. Raw harmonic images obtained by (a) LC laser with t_{delay} of NIP at -1.6 ps and (b) HC laser with t_{delay} of coaxial prepulse at -4 ps [optimal (opt) scale length]. (c) Harmonic spectra drawn from (a), Fig. 1(b), and (b). (d) Dependence of the integrated intensity of harmonics (15th–20th) on the t_{delay} of NIP. The red and green stripes show the experimental harmonic intensities for the HC case and the HC-opt case, respectively. Numerical simulation results are also plotted for comparison.

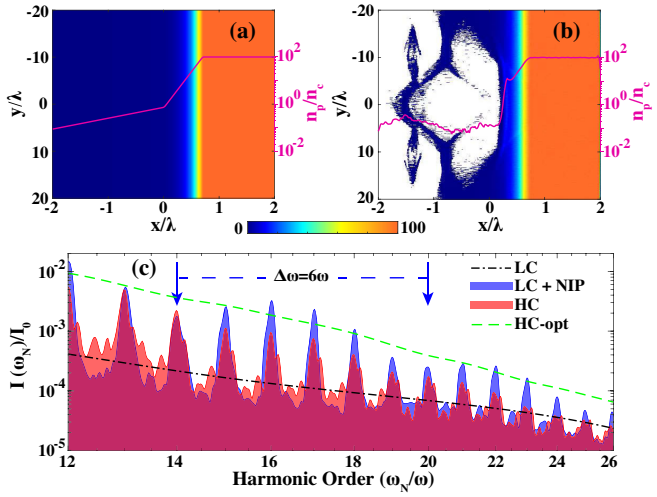

FIG. 3. Simulated 1D (red lines) and 2D (colored images) plasma density distributions at (a) $t = 0$ and (b) $t = 1.6$ ps. The plasma density is normalized by n_c. (c) Simulated harmonic spectra under four different preplasma conditions. The black dashed and green dash-dotted lines are the spectral envelopes for the LC laser and the HC laser with optimum scale length ($L = 0.08\lambda$), respectively. The red and blue areas show the harmonic spectra for HC laser ($L = 0.05\lambda$) and with the compressed surface in (b), respectively. The harmonic intensity is normalized by $I_0 = 2.15 \times 10^{18}$ W/cm^2.

preplasma could be controlled by t_{delay}. The experimental results showed that the efficiency of HHG was higher when the coaxial prepulse was added to generate a slightly larger L. The harmonic intensity reached its maximum when t_{delay} was -4 ps; the raw harmonic image and its spectrum are shown in Figs. 2(b) and 2(c), respectively. One can see that the intensity of each harmonic generated with the optimized scale length is enhanced compared to that generated by the HC laser alone. However, the harmonic spectrum always declines monotonically by HC lasers with varied scale lengths.

According to the similarity theory of ROM mechanism [3], the spectral shape should be similar if the similarity parameter $S = n_e/a_0 n_c$ (n_e the electron density at the laser reflection surface and a_0 the dimensionless electromagnetic potential of laser) remains constant. For the preplasma with a continuous density ramp, the laser is always reflected at the critical density surface even though the plasma scale length is changed. Therefore, the harmonic intensity changes, but the spectral shape remains similar. The plateau profile of harmonics generated by the LC + NIP lasers indicates that the plasma surface becomes overcritical due to the NIP compression, and thus the S parameter is modified. Our previous study showed that if the plasma is truncated at $n_e > n_c$, harmonic pulses will be emitted multiple times in a laser cycle due to the high-mode oscillations of surface electrons [17]. This causes the envelope of harmonic spectrum to be modulated, and the spectral width of each harmonic gets narrower, as shown in our experimental observation in Figs. 2(a) and 2(c). In addition, we observed that the experimental harmonic intensity obtained by the LC + NIP lasers depends on the t_{delay} of NIP. As shown in Fig. 2(d), the integrated intensity of the 15th–20th harmonics reaches a maximum at $t_{\mathrm{delay}} = -1.6$ ps. This intensity is comparable to that obtained by the HC laser with the optimum scale length.

To understand the efficient HHG via surface plasma compression, we performed particle-in-cell (PIC) simulations. We first investigated the evolution of preplasma when the NIP was introduced. According to the hydrodynamic simulation result (LC) in Fig. 1(c), the preplasma in the PIC simulations was initially set to be double scaled with $L = \lambda$ followed by $L = 0.15\lambda$. The kick point of the plasma density was at the critical density n_c. Figure 3(a) shows the initial one-dimensional (1D) and two-dimensional (2D) plasma density distributions. The plasma consists of electrons and fully ionized Si^{14+} with an initial temperature of 10 eV. Both electrons and ions are mobile. The simulation box is set to $x \times y = 7\lambda \times 44\lambda$ with 700×4400 grids. To suppress the numerical noise, each grid contains 144 macroelectrons and 36 macroions. A circularly polarized laser with a pulse shape of $a = a_0 \sin^2(\pi t/2\tau)\exp(-y^2/w_0^2)$ is normally incident from the left boundary of the simulation box, where $a_0 = 0.3$, $\tau = 10\ T_0$, and $w_0 = 12\lambda$ are taken from the parameters of the NIP used in the experiment. The simulated preplasma density distributions at $t =$ 1.6 ps are shown in Fig. 3(b). A curved surface with a width of 18λ and a depth of 0.08λ can be observed on the 2D density map. The curved surface forms rapidly after the irradiation of the NIP due to its radiation pressure, which pushes the low-density plasma toward the target surface. The 1D profile shows clearly that the preplasma is

compressed into a sharp truncation around $x = 0$ with an overcritical density of $12n_c$. Simulations also show that the truncation density can be tuned by the NIP intensity, and the curvature of the compressed surface is related to the pulse intensity and beam waist of the NIP.

We then explain the plateau profile in Fig. 2(c) with a simplified plasma distribution, where the underdense part before the curved surface in Fig. 3(b) is removed. The curved surface can be approximated as $|y(x)| = 32\sqrt{-x}$, where $x = 0$, $y = 0$ is the central position of the surface with a cutoff density of $n_p = 12n_c$. Beyond this parabolic surface, the plasma density increases exponentially with $L = 0.15\lambda$, which is unaffected by the NIP. Similar to the experiment, the peak amplitude of the main pulse is $a_0 = 4$, and the incidence angle is 45°. The pulse duration is $\tau = 10T_0$, and the beam waist is $w_0 = 6\lambda$. Figure 3(c) shows the harmonic spectra obtained from the 2D simulations. The spectrum with the NIP-compressed surface exhibits a broad modulation with $\Delta\omega = 6\omega$. Harmonics among each modulation are enhanced. The simulation reproduces the experimental spectral features shown in Fig. 2(c). The reason for harmonic enhancement with preplasma truncation is that the electrons on such edged surface are simultaneously driven by the electromagnetic force (ω) and ponderomotive force (2ω) of the laser pulse [27]. The truncation of low-density preplasma by NIP enables the laser to drive surface electron oscillations more efficiently.

Harmonic generations with changed conditions similar to the experiment are also simulated, and compared in Fig. 3(c). Note that when the plasma mirror is applied, the laser intensity reduces to $a_0 = 3.5$. We can observe that the lowest harmonic generation efficiency is obtained with a LC laser. The harmonic intensity increases significantly with a HC laser ($L = 0.05\lambda$) but is still lower than that with the NIP compression. Simulations show that the $L = 0.05\lambda$ produced by a HC laser is not optimal for HHG. The harmonic intensity could be further increased by tuning the scale length to $L = 0.08\lambda$, as shown in Fig. 3(c), which was achieved by introducing a coaxial prepulse with a suitable t_{delay} in the experiment. In the simulation results, we can also observe that the harmonic spectrum using the HC laser always declines monotonically, although a small change in the plasma scale length greatly affects the harmonic generation efficiency. Only the harmonic spectrum obtained by a LC laser with the NIP compression presents a plateau profile with some modulation among the harmonic orders.

Simulations have generally shown good agreement with our experimental observations for efficient HHG. There are also some fine differences between the experimental and simulation results. As shown in Fig. 2(b), the harmonics are split in the experimental observation, which is not observed in the simplified simulation result in Fig. 3(c). In addition, the experimental harmonic intensity in the LC + NIP case

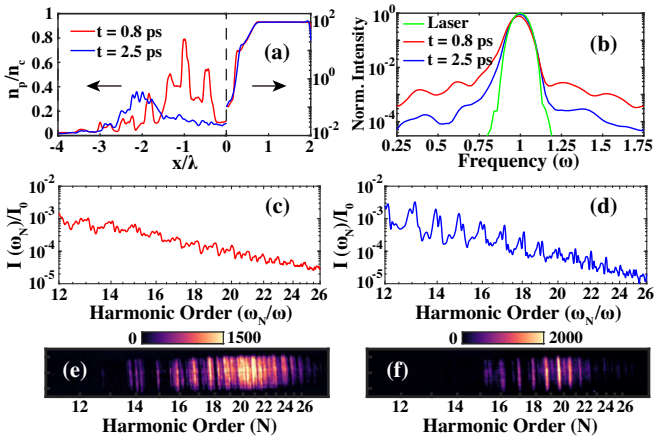

FIG. 4. (a) Simulated 1D plasma density profiles at two different moments after the NIP compression. (b) Laser spectral evolution after passing through the low-density pedestal in (a). Harmonic spectra obtained by 2D PIC simulations with the plasma profiles at $t = 0.8$ ps (c) and $t = 2.5$ ps (d). Corresponding to the simulation results, harmonic spectral images obtained in the experiment when the t_{delay} of NIP is -0.8 ps (e) and -2.5 ps (f).

depends on the t_{delay} of NIP, as shown in Fig. 2(d). We verified by simulations that the dependence of harmonic intensity on t_{delay} and these spectral splits were both caused by the plasma evolution before the curved surface. During the NIP radiation, a fraction of the NIP energy is trapped in the long low-density preplasma owing to the interaction of the NIP and its reflected pulse with the ambient plasma, which forms bubblelike structures, as shown in Fig. 3(b). PIC simulations show that the curved surface can survive for a much longer duration than the bubbles. As the trapped laser energy dissipates, the plasma density around these bubbles gradually decreases and forms an underdense pedestal.

Figure 4(a) show the simulated 1D plasma profiles at $t = 0.8$ ps and $t = 2.5$ ps after the NIP compression. Both 1D and 2D PIC simulations were performed, and the calculated plasma profiles along the target normal are similar. A high plasma pedestal can be observed at the early stages. However, the pedestal density becomes relatively low as time goes; meanwhile the target surface becomes less sharp. Figure 4(b) shows the modification of laser spectrum after passing through the plasma pedestal. It can be seen that the laser spectrum is broadened and shows a few sideband components. This should be due to the relativistic self-phase modulation [12]. For a higher pedestal, the spectral modification of laser is more significant. These sideband components indicate variation in the drive laser waveform, which affects the radiation time and profile of HHG, imposing significant influence on harmonic spectrum. The harmonic spectra obtained with the density distributions referring to Fig. 4(a) are presented in Fig. 4(c) ($t = 0.8$ ps) and Fig. 4(d) ($t = 2.5$ ps). Harmonics with a

high pedestal are irregularly split [Fig. 4(c)], and the spectral intensity is lower compared with that in Fig. 3(c). Figure 4(e) is the experimental harmonic image when the t_{delay} of NIP is −0.8 ps. Severely harmonic splitting can also be observed in the image. The low pedestal causes relatively weak sideband components of laser, and thus weak harmonic splitting [Fig. 4(d)]. The experimental spectrum [Fig. 4(f)] also shows no obvious split harmonic when the t_{delay} of NIP is −2.5 ps. The dependence of simulated harmonic intensity on t_{delay} is also shown in Fig. 2(d). The reduction of harmonic intensity with a larger t_{delay} is mainly due to the reexpansion of the compressed surface, which decreases the effective plasma density for HHG. These results verify that efficient harmonic generation by surface plasma compression can be obtained in a temporal window of t_{delay} when both a sharp plasma surface and a low plasma pedestal are formed.

In conclusion, through experiments and simulations, we have demonstrated that efficient HHG from relativistic laser-solid interaction can be achieved via compressing surface plasma to overcritical density with a sharp front. The harmonic intensity obtained by this method is comparable to that obtained by optimizing the plasma scale length. Surface plasma compression is driven actively by a circularly polarized NIP, even with low-contrast lasers. Our NIP-assisted scheme may pave a way for high repetition rate EUV sources with high brightness for various applications. Such sources are being pursued in this field and different schemes have been proposed [28]. Moreover, our studies also reveal that the preplasma can be tailored into a curved surface using the radiation pressure of NIP. This may also be an efficient way to focus relativistic harmonics [29] or to produce high-order vortex harmonics [30].

The simulations are performed on the Π Supercomputer Center at SJTU. This work was supported by the National Natural Science Foundation of China (Grants No. 11905129, No. 12175140, No. 11991074, and No. 12135009), and the Strategic Priority Research Program of the Chinese Academy of Sciences (Grants No. XDA25010500 and No. XDA25050000).

*liuf001@sjtu.edu.cn
†minchen@sjtu.edu.cn

[1] P. Gibbon, Phys. Rev. Lett. **76**, 50 (1996).
[2] R. Lichters, J. Meyer-ter-Vehn, and A. Pukhov, Phys. Plasmas **3**, 3425 (1996).
[3] T. Baeva, S. Gordienko, and A. Pukhov, Phys. Rev. E **74**, 046404 (2006).
[4] D. Popmintchev *et al.*, Phys. Rev. Lett. **120**, 093002 (2018).
[5] A. Ravasio *et al.*, Phys. Rev. Lett. **103**, 028104 (2009).
[6] J. A. Wheeler, A. Borot, S. Monchocé, H. Vincenti, A. Ricci, A. Malvache, R. Lopez-Martens, and F. Quéré, Nat. Photonics **6**, 829 (2012).
[7] G. Lambert *et al.*, Nat. Phys. **4**, 296 (2008).
[8] S. Gordienko, A. Pukhov, O. Shorokhov, and T. Baeva, Phys. Rev. Lett. **94**, 103903 (2005).
[9] M. Zepf *et al.*, Phys. Rev. E **58**, R5253 (1998).
[10] S. Kahaly, S. Monchocé, H. Vincenti, T. Dzelzainis, B. Dromey, M. Zepf, Ph. Martin, and F. Quéré, Phys. Rev. Lett. **110**, 175001 (2013).
[11] F. Dollar, P. Cummings, V. Chvykov, L. Willingale, M. Vargas, V. Yanovsky, C. Zulick, A. Maksimchuk, A. G. R. Thomas, and K. Krushelnick, Phys. Rev. Lett. **110**, 175002 (2013).
[12] I. Watts, M. Zepf, E. L. Clark, M. Tatarakis, K. Krushelnick, A. E. Dangor, R. Allott, R. J. Clarke, D. Neely, and P. A. Norreys, Phys. Rev. E **66**, 036409 (2002).
[13] J. Gao *et al.*, Chin. Opt. Lett. **15**, 081902 (2017).
[14] M. Cerchez, R. Prasad, B. Aurand, A. L. Giesecke, S. Spickermann, S. Brauckmann, E. Aktan, M. Swantusch, M. Toncian, T. Toncian, and O. Willi, High Power Laser Sci. Eng. **7**, e37 (2019).
[15] C. Rodel *et al.*, Phys. Rev. Lett. **109**, 125002 (2012).
[16] J. P. Geindre, P. Audebert, and R. S. Marjoribanks, Phys. Rev. Lett. **97**, 085001 (2006).
[17] B. Y. Li, F. Liu, M. Chen, Z. Y. Chen, X. H. Yuan, S. M. Weng, T. Jin, S. G. Rykovanov, J. W. Wang, Z. M. Sheng, and J. Zhang, Phys. Rev. E **100**, 053207 (2019).
[18] X. L. Ge *et al.*, Chin. Opt. Lett. **16**, 103202 (2018).
[19] See Supplemental Material at http://link.aps.org/supplemental/10.1103/PhysRevLett.128.244801 for the reproducibility of harmonic generation via surface plasma compression, the method of adding coaxial prepulse, and addition information, which includes Refs. [18, 20–23].
[20] O. Willi *et al.*, Plasma Phys. Controlled Fusion **51**, 124049 (2009).
[21] S. C. Wilks, W. L. Kruer, M. Tabak, and A. B. Langdon, Phys. Rev. Lett. **69**, 1383 (1992).
[22] F. Quere, C. Thaury, P. Monot, S. Dobosz, Ph. Martin, J.-P. Geindre, and P. Audebert, Phys. Rev. Lett. **96**, 125004 (2006).
[23] N. V. Didenko, A. V. Konyashchenko, A. P. Lutsenko, and S. Y. Tenyakov, Opt. Express **16**, 3178 (2008).
[24] C. Thaury *et al.*, Nat. Phys. **3**, 424 (2007).
[25] R. Ramis, and J. Meyer-ter-Vehn, Comput. Phys. Commun. **203**, 226 (2016).
[26] M. Behmke *et al.*, Phys. Rev. Lett. **106**, 185002 (2011).
[27] I. Watts, M. Zepf, E. L. Clark, M. Tatarakis, K. Krushelnick, A. E. Dangor, R. M. Allott, R. J. Clarke, D. Neely, and P. A. Norreys, Phys. Rev. Lett. **88**, 155001 (2002).
[28] See for example, A. Borot, A. Malvache, X. Chen, D. Douillet, G. Iaquianiello, T. Lefrou, P. Audebert, J.-P. Geindre, G. Mourou, F. Quéré, and R. Lopez-Martens, Opt. Lett. **36**, 1461 (2011); S. Mondal *et al.*, J. Opt. Soc. Am. B **35**, A93 (2018); A. Tarasevitch, K. Lobov, C. Wunsche, and D. von der Linde, Phys. Rev. Lett. **98**, 103902 (2007); J. Bierbach *et al.*, New J. Phys. **14**, 065005 (2012).
[29] H. Vincenti, Phys. Rev. Lett. **123**, 105001 (2019).
[30] J. W. Wang, M. Zepf, and S. G. Rykovanov, Nat. Commun. **10**, 5554 (2019).